N O T I C E

THIS DOCUMENT HAS BEEN REPRODUCED FROM MICROFICHE. ALTHOUGH IT IS RECOGNIZED THAT CERTAIN PORTIONS ARE ILLEGIBLE, IT IS BEING RELEASED IN THE INTEREST OF MAKING AVAILABLE AS MUCH INFORMATION AS POSSIBLE

77-224

FINAL REPORT

A SYSTEM DEFINITION STUDY FOR THE ADVANCED METEOROLOGICAL TEMPERATURE SOUNDER (AMTS)

Contract No. 954787

For - Jet Propulsion Laboratory
4800 Oak Grove Drive
Pasadena, California 91103

SANTA BARBARA RESEARCH CENTER · SBRC

A Subsidiary of Hughes Aircraft Company

SANTA BARBARA RESEARCH CENTER

A Subsidiary of Hughes Aircraft Company

75 COROMAR DRIVE, GOLETA, CALIFORNIA

FINAL REPORT

A SYSTEM DEFINITION STUDY FOR THE ADVANCED METEOROLOGICAL TEMPERATURE SOUNDER (AMTS)

Contract No. 954787

for

Jet Propulsion Laboratory
4800 Oak Grove Drive
Pasadena, California 91103

October 1977

SANTA BARBARA RESEARCH CENTER

A Subsidiary of Hughes Aircraft Company

75 COROMAR DRIVE, GOLETA, CALIFORNIA

FINAL REPORT

A SYSTEM DEFINITION STUDY FOR THE ADVANCED METEOROLOGICAL TEMPERATURE SOUNDER (AMTS)

Contract No. 954787

for

Jet Propulsion Laboratory
4800 Oak Grove Drive
Pasadena, California 91103

October 1977

ILLUSTRATIONS

ILLUSTRATIONS

PRECEDING PAGE BLANK NOT FILMED

TABLES

INTRODUCTION

The Advanced Meteorological Temperature Sounder (AMTS) Definition Study was conducted in essential conformance with Jet Propulsion Laboratory Contract 954787. Specifically, the functional requirements of Exhibit A (II) were used as the baseline for the conceptual design of a fixed grating out-of-plane multi-detector spectrometer for the Space Shuttle application.

While the main emphasis of the study was placed on spectrometer design and performance, it was apparent that the grating instrument would be large and the 28 element detector array could be difficult to cool radiatively from a free flying spacecraft. Further, it was recognized that increasing the spectral resolution of the grating instrument would be difficult in an instrument of reasonable size.

For these reasons a parallel study of a Michelson interferometer spectrometer was undertaken. This type of instrument offers compact size, fewer detectors to cool, and the possibility of increased spectral resolution.

In this connection a company-funded development of a laboratory interferometer based on the AMTS requirements has been started.

This study report contains the design and performance parameters of both the grating and interferometer approaches, and in addition discusses the tradeoffs involved in comparing the two systems for sounding applications.

SYSTEM REQUIREMENTS

The requirements contained in this section were derived from Section II, Exhibit A of the contract as modified by discussions and communications with JPL personnel.

1. Wavelength Channels - Table 1 lists the wavelengths of each of the twenty-eight channels together with the maximum and minimum expected scene temperatures and minimum signal-to-noise ratios (SNRs) required for each channel.

2. Radiometric Accuracy - Absolute radiometric accuracy ±1% in all channels.

3. Scan Pattern and Field of View - The instrument scans ±45° along a line perpendicular to the ground track. The instrument footprint is 45 km × 45 km at nadir including smear of the scanned spectrometer slit. These requirements are the same for both the 417-km Space Shuttle orbit and the free flyer altitude of approximately 900 km.

3a. Field-of-View Simultaneity - The spatial registration and sampling of all spectral channels must be such that the difference in surface area covered is less than 1% (1σ). Factors affecting registration could be spacecraft or scan motion during sampling or field-of-view (FOV) misregistration in the optical system.

4. Signal-to-Noise - (See Table 1.)

5. Dynamic Range - (See Table 1.)

6. Crosstalk - The maximum permissible combined electrical and optical crosstalk between any two detector channels shall be less than 0.1%.

7. Operating Environment - Space Shuttle nominal orbit altitude and inclination as defined in Space Shuttle System Payload Accommodation, JSC 07700, Vol. 14, Rev. 16, November 1975, and subsequent updates.

8. Time in Orbit - Up to two weeks.

Table 1. AMTS Channel Requirements

CHANNEL NO.	ν^{**} (cm^{-1})	$\Delta\nu$ (cm^{-1})	T_{max} ($^\circ$K)	T_{min} ($^\circ$K)	SNR (min)	MAIN FUNCTION
1	607.00	0.5	288	216	100	CLOUDS
2	623.23	0.5	276	214	100	CLOUDS
3	627.75	0.5	246	213	100	CLOUDS
4	635.80	0.5	230	212	100	TEMPERATURE
5	646.65	0.5	228	210	100	TEMPERATURE
6	652.75	0.5	229	207	100	TEMPERATURE
7	666.20	0.5	233	209	100	TEMPERATURE
8	666.90	0.5	233	209	100	TEMPERATURE
9	668.10	0.5	254	220	100	TEMPERATURE
10	669.10	0.5	242	213	100	TEMPERATURE
11	1203.00	1.0	320	216	100	CLOUDS
12	1231.80	1.0	320	216	100	CLOUDS
13	1772.00	1.5	250	216	100	HUMIDITY
14	1844.50	1.5	250	216	100	HUMIDITY
15	1889.50	1.5	250	216	100	HUMIDITY
16	1809.50	1.5	250	216	100	HUMIDITY
17	1839.40	1.5	270	216	100	HUMIDITY
18	1850.90	1.5	280	216	100	HUMIDITY
19	1930.10	1.5	320	216	100	HUMIDITY
20	2383.75	2.0	237	214	100	TEMPERATURE
21	2386.10	2.0	257	214	100	TEMPERATURE
22	2388.20	2.0	274	215	100	TEMPERATURE
23	2390.20	2.0	292	215	100	TEMPERATURE
24	2392.35	2.0	306	217	100	TEMPERATURE
25	2394.50	2.0	306	217	100	TEMPERATURE
26	2424.00	2.5	320	214	$^\circ$	SURFACE TEMP
27	2505.00	2.5	320	214	$^\circ$	SURFACE TEMP
28	2616.50	2.5	320	214	$^\circ$	SURFACE TEMP

$^\circ$THE MINIMUM ACCEPTABLE SIGNAL-TO-NOISE RATIOS FOR THESE CHANNELS MAY BE LOWER THAN 100 SINCE THEY VIEW CLOSE TO THE EARTH SURFACE.

**WAVELENGTH TOLERANCE - KNOWLEDGE $\pm 0.1\Delta\nu$; STABILITY $\pm 0.02\Delta\nu$

ORBITAL PARAMETERS

Table 2 gives the orbital parameters for the conditions stated above as a function of spacecraft altitude.

Table 2. Orbital Parameters

h (km)	a x 10^8 (cm)	P (min)	α (45 km) (rad)	V_0 (km/sec)	V_g (km/sec)	T_L (sec)	T_D (sec)	Δf_n (Hz)	DOWN TRACK SMEAR	
									(km)	% FOOTPRINT
350	6.73	91.4	0.128	7.71	7.31	3.69	0.302	1.65	2.21	4.9
400	6.78	92.4	0.112	7.68	7.23	3.73	0.267	1.87	1.93	4.3
417°	6.79	92.74	0.108	7.67	7.20	3.75	0.258	1.94	1.86	4.1
500	6.88	94.45	0.09	7.63	7.07	3.82	0.219	2.28	1.55	3.4
700	7.08	98.6	0.064	7.52	6.77	3.98	0.163	3.07	1.10	2.5
800	7.18	100.7	0.056	7.46	6.63	4.07	0.146	3.42	0.97	2.2
900°°	7.28	102.8	0.050	7.41	6.49	4.16	0.132	3.79	0.86	1.9
1000	7.38	104.93	0.045	7.36	6.36	4.24	0.121	4.13	0.77	1.7

WHERE
- h · ORBITAL ALTITUDE
- a · ORBITAL RADIUS REFERRED TO EARTH CENTER
- P · ORBITAL PERIOD
- α · IFOV OF 45 km FOOTPRINT AT NADIR
- V_0 · ORBITAL VELOCITY
- V_g · VELOCITY OF FOOTPRINT AT NADIR
- T_L · LINE TIME (±45°)
- T_D · DWELL TIME OF IFOV
- Δf_n · EQUIVALENT NOISE BANDWIDTH · $\frac{1}{2T_D}$

°ASSUMED SHUTTLE ALTITUDE
°°ASSUMED FREE FLYER ALTITUDE

BASELINE SYSTEM

The instrument used as the baseline in this study is an out-of-plane
Ebert-Fastie grating mount used in multiple orders (M=1, 2, 3, 4). The sys-
tem is shown schematically in Figure 1, and the design parameters are given
in Table 3.

Table 3. Grating Spectrometer Design Parameters

SOLID ANGLE-AREA PRODUCT	$\Omega A = 0.01$ sr-cm^2
FOCAL RATIO	f/3.5 "SQUARE"
FOCAL LENGTH	43.3 cm
GRATING ANGLE	57°
OUT-OF-PLANE ANGLE	16°
GRATING SPACING	0.00095 cm
ENTRANCE SLIT DIMENSIONS	1.25 cm x 0.125 cm
EXIT SLIT DIMENSIONS	(SEE TABLE 5)
GRATING ORDERS	1, 2, 3, 4

In this system the fore optics operate at $A\Omega = 0.01$, a value close to the
maximum possible for a reasonable grating spectrometer design. The fore
optics are designed to give the desired footprint which is an image of the en-
trance slit 45 km × 4.5 km on the earth. Since this same footprint size is
desired irrespective of spacecraft altitude, the aperture and focal length of
the fore optics must be changed as a function of altitude to give constant $A\Omega$
and constant entrance slit dimensions. For the shuttle altitude case being
considered, aperture diameter is 3.3 cm and the focal ratio is f/3.5. The
free flyer altitude of 900 km would require a larger aperture of 7.1 cm.

For purposes of this study it is assumed that the fore optics can be a
simple off-axis paraboloid. In any case, the image quality degradation of
the fore optics will be small compared to that of the spectrometer itself owing
to the FOV size (6.2° × 0.62°).

The chopper is located close to the focal plane ahead of the entrance
slit. It will be a resonant fork type operating at about 500 Hz, a value chosen
to be above the 1/f noise knee frequency for the HgCdTe detectors.
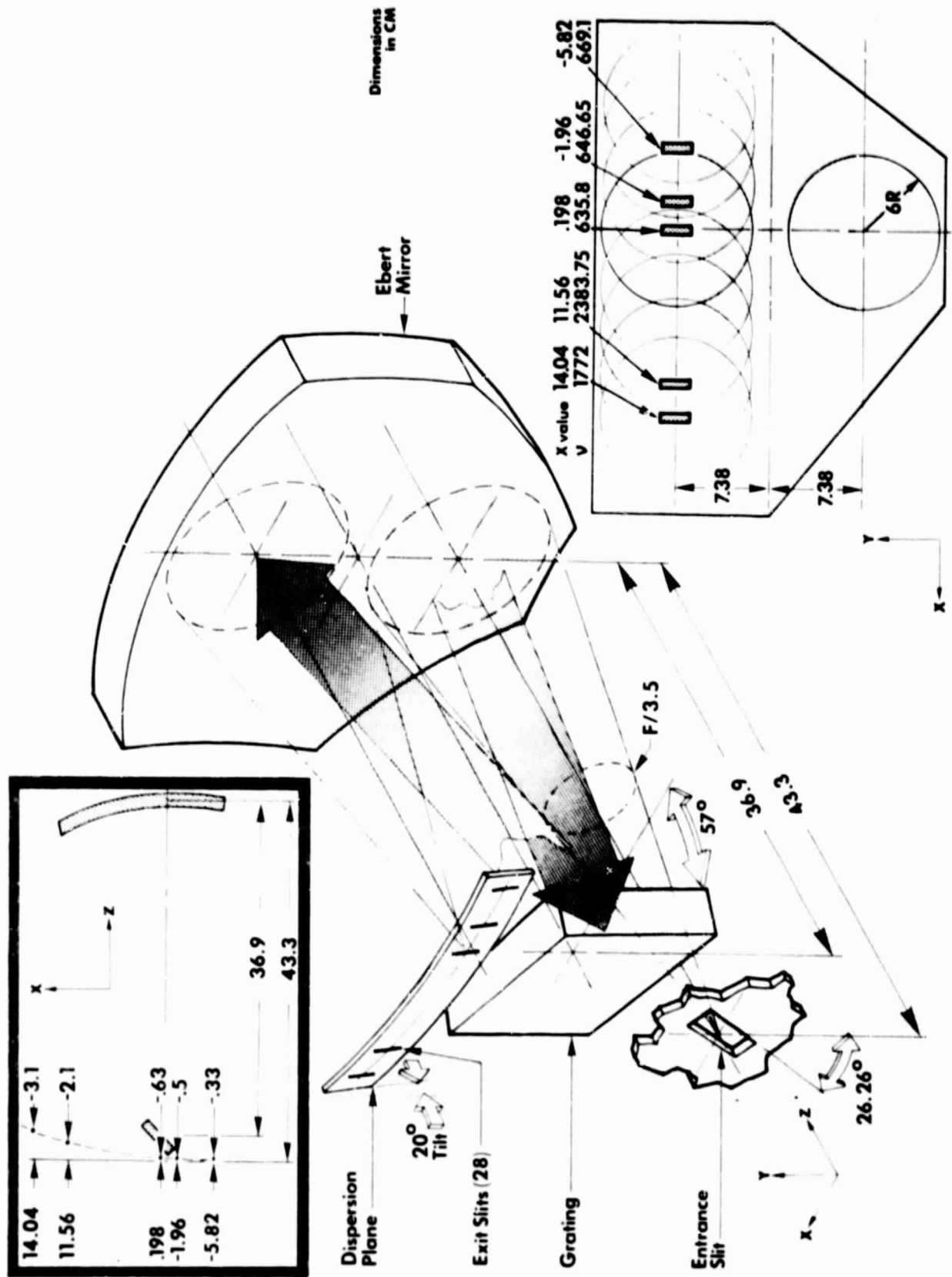
Figure 1. AMTS Grating Spectrometer Conceptual Drawing

Scanning is produced by a small object-space plane mirror mounted at 45° to a shaft parallel to the optical axis. The data in Table 2 are based on consecutive scan swaths that are contiguous at the nadir. Dwell time, T_D, is the time required for the footprint (45 km × 45 km) to traverse its dimension on the ground. The footprint is generated by scanning the image of the entrance slit which is 45 km in the along-track direction and 4.5 km in the across-track direction.

Scanning is continuous, and to ensure spatial simultaneity hold-sample-and-dump circuits are used for each channel. Integrators are proposed for the channel output circuits to ensure independence of consecutive data samples.

The scan system as described has the advantage that by rotating the mirror shaft the system can be made to view the earth, space for dc restoration, and one or more blackbody references. However, the scan produces image rotation equal to the mirror angle away from nadir. Thus, at the ends of the 45° scan swath the entrance slit image will appear rotated 45°. In terms of area coverage, however, the foreshortening effect of the image rotation will be almost perfectly matched by the increase in footprint size at the ends of scan (for a flat earth the match would be perfect). Figure 2 shows the deviation of the footprint size from the nominal 45-km dimension as a function of scan angle.
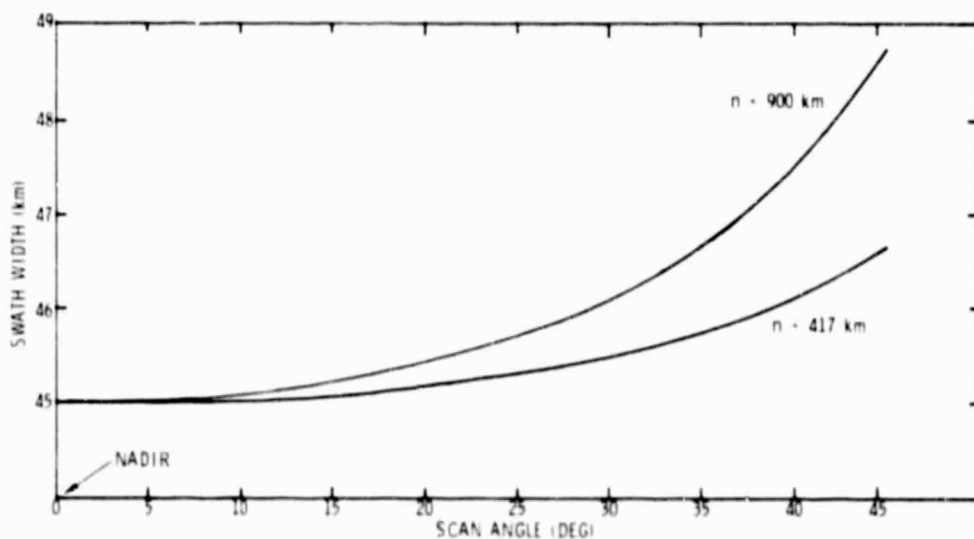
Figure 2. Swath Width versus Scan Angle

SPECTROMETER DESIGN

In this system the scene is imaged at the entrance slit which therefore determines the instantaneous field of view (IFOV). The entrance slit is imaged at the exit slit. The disperson angle β has been made equal to the grating angle α for the channel near the center of the frequency range in the first order. For this channel (637.24 cm^{-1}), the exit slit is equal in width to the entrance slit. All other exit slits are either larger or smaller than the $\alpha = \beta$ case depending on which side of the $\alpha = \beta$ exit slit they are on and the grating order.

The entrance aperture is imaged on the grating and the grating in turn would be imaged on the detector were it not for condensing light pipes located immediately behind each of the spherical field lenses. Each lens is a rectangular "sliver" corresponding in aspect ratio to the exit slit it is behind and each operates f/1 in the plane of its long dimension. The light pipe which has reflecting sides only on the faces adjoining the long lens dimension reduces the detector dimension by a factor of three. Therefore, the detector has an aspect ratio of about three.

The most important property of this anamorphic optical system is that it reduces the detector width such that the detectors can be mounted on the detector plane without overlapping. This is illustrated in Figure 3. A secondary feature is that the area of the detectors is reduced thereby reducing detector noise.

The equations used to describe spectrometer operation are as follows:

$$\frac{m}{\nu} = a \cos \delta \, (\sin \alpha + \sin \beta) \tag{1}$$

where m is the order = 1, 2, 3, 4

   ν is the frequency in cm^{-1}

   δ is the out-of-plane angle = 10°

   α is the grating angle = 57°

   β is the dispersion angle (see Table 4)
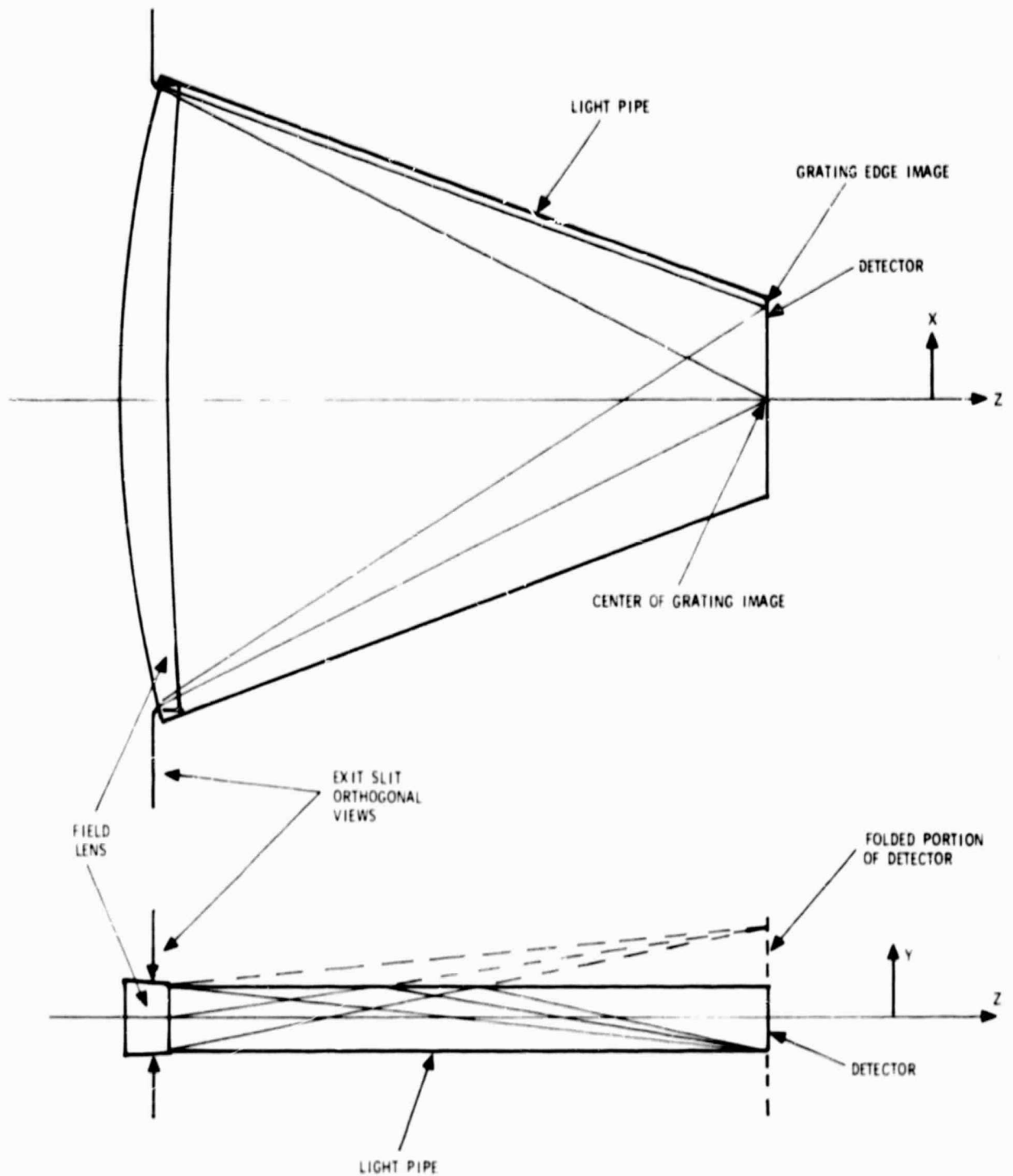
Figure 3. Anamorphic Field Lens-Light Pipe Schematic

Table 4. Grating Spectrometer System Parameters

CHANNEL	ν (cm⁻¹)	$\nu/\Delta\nu$	β (deg)	S_W (cm)	S_L (cm)	d_W (cm)	d_L (cm)	A_D (cm²)
1	607.00	1214.0	67.26	0.162	1.25	0.0384	0.357	0.0
2	623.23	1246.5	61.21	0.124	1.25	0.0365	0.357	0.0130
3	627.75	1255.5	59.77	0.117	1.25	0.0359	0.357	0.0128
4	635.80	1271.6	57.40	0.106	1.25	0.0350	0.357	0.0125
5	646.65	1293.3	54.51	0.095	1.25	0.0339	0.357	0.0121
6	652.75	1305.5	53.02	0.090	1.25	0.0332	0.357	0.0119
7	666.20	1332.4	49.97	0.0811	1.25	0.0319	0.357	0.0114
8	666.90	1333.8	49.82	0.081	1.25	0.0318	0.357	0.0114
9	668.10	1336.2	49.57	0.080	1.25	0.0317	0.357	0.0113
10	669.10	1338.2	49.36	0.079	1.25	0.0316	0.357	0.0113
11	1203.0	1203.0	69.77	0.185	1.25	0.0391	0.357	0.0140
12	1231.80	1231.8	63.74	0.138	1.25	0.0373	0.357	0.0133
13	1772.00	1181.3	76.15	0.277	1.25	0.0406	0.357	0.0145
14	1844.50	1229.7	64.13	0.140	1.25	0.0375	0.357	0.0134
15	1889.50	1259.7	59.14	0.114	1.25	0.0357	0.357	0.0127
16	1809.50	1206.3	68.98	0.177	1.25	0.0389	0.357	0.0139
17	1839.40	1226.3	64.77	0.144	1.25	0.0377	0.357	0.0134
18	1850.90	1233.9	63.35	0.136	1.25	0.0372	0.357	0.0133
19	1930.10	1286.7	55.36	0.098	1.25	0.0342	0.357	0.0122
20	2383.75	1191.9	72.73	0.217	1.25	0.0399	0.357	0.0142
21	2386.10	1193.0	72.39	0.215	1.25	0.0398	0.357	0.0142
22	2388.20	1194.1	72.10	0.211	1.25	0.0397	0.357	0.0142
23	2390.20	1195.1	71.82	0.201	1.25	0.0397	0.357	0.0142
24	2392.35	1196.2	71.53	0.204	1.25	0.0396	0.357	0.0141
25	2394.50	1197.3	71.24	0.201	1.25	0.0395	0.357	0.0141
26	2424.0	969.6	67.69	0.207	1.25	0.0482	0.357	0.0172
27	2505.0	1002	60.24	0.149	1.25	0.0451	0.357	0.0161
28	2616.5	1046.6	52.69	0.112	1.25	0.0414	0.357	0.0147

WHERE $\nu/\Delta\nu$ = CHANNEL SPECTRAL RESOLUTION
  β = DISPERSION ANGLE
  S_W = EXIT SLIT WIDTH
  S_L = EXIT SLIT LENGTH
  d_W = DETECTOR WIDTH
  d_L = DETECTOR LENGTH
  A_D = DETECTOR AREA

$$S_w = \frac{\sin\alpha + \sin\beta}{\cos\beta} \frac{f}{(\nu/\Delta\nu)} \qquad (2)$$

where S_w is the width of the exit slit

  f is the focal length of the spectrometer

  $\nu/\Delta\nu$ is the channel resolution

The detector dimension across the narrow side is determined by:

$$S_d = \frac{S_{w_4}}{3} \frac{\cos\beta_n}{\cos\beta_4} \qquad (3)$$

The width of the entrance slit, S_w, is determined by the relation

$$A\Omega = \frac{S_w S_L}{(f/\#1)(f/\#2)} = 0.01 \qquad (4)$$

SANTA BARBARA RESEARCH CENTER

where S_L is the length of the entrance slit, f/#1 and f/#2 are the focal ratios of the telescope and spectrometer, respectively, (both are f/3.5), and $S_L = 10 S_w$.

The grating size is such that it appears "square" for the $\alpha = \beta$ case, and over or under square for smaller or larger values of β. Equation (3) corrects for this effect and reduces the detector dimension, S_w, by a factor of 3 to account for the condensing light pipe.

Values from equations (1), (2) and (3) are given in Table 4.

Spectrometer Slit Functions

The slit functions for the AMTS grating spectrometer were derived from a combination of ray trace data and convolution with geometric slit functions. For purposes of these calculations, the entrance slit is rotated $26°$ from a line parallel to the grating lines.

At the exit slit plane, the slits are inclined $20°$ to maintain reasonable focus along the length of the slit. Although the exact value varies slightly for each slit, this is a reasonable compromise.

196 rays are traced from each of three object points on the entrance slit, the center of the slit and ± 0.67 of the slit length (2/3 distribution to end of slit), such that it may be considered that each spot diagram represents 1/3 of the slit length. This selection avoids some of the worst rays at the very end of the slit, but provides a sensible average of energy distribution.

The energy distribution from the three field points is analyzed by "in effect" passing a slit across the image and counting the number of rays at each slit position. The step size or width of the slit is selected to be a fraction of the exit slit desired. The net effect of this is that some approximations are used which are not exactly commensurate with the design exit slit or entrance slit widths. The parameters used for each of the five exit slits covering the length of the exit slit plane are given in Table 5.

Table 5. Exit Slit Parameters

BAND	STEP WIDTH FOR SPOT DIAGRAM ANALYSIS	STEPS IN ENTRANCE SLIT CONVOLUTION	EFFECTIVE ENTRANCE SLIT USED	STEPS IN EXIT SLIT CONVOLUTION	EFFECTIVE EXIT SLIT WIDTH
635.8	0.0158	10	0.158	10	0.158
646.65	0.015	10	0.15	10	0.15
669.1	0.015	10	0.15	8	0.12
1772	0.032	5	0.16	10	0.320
2383.7	0.032	5	0.16	9	0.288

The convolution is done with a desk calculator, first combining the entrance slit with the image, and then combining the exit slit. The technique is much like finding a moving average over a fixed number of units.

Five slit functions were calculated as described. These are shown in Figures 4 through 8.

The exit slit plane is steeply curved owing to the short focal length of the spectrometer. This configuration was driven by the need for the smallest possible detector array size (to minimize radiative cooler heat load). A schematic drawing of the exit slit plane is shown in Figure 1.

For the Space Shuttle application such a compact design would not be needed since the detectors could be cooled by other means (for example a liquid nitrogen transfer system or a Joule-Thomson cryostat system).
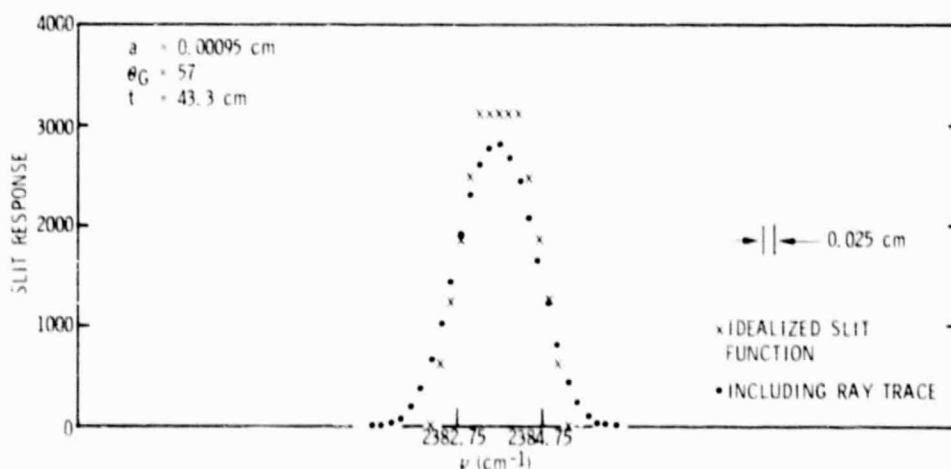
Figure 4. Slit Response Function ($\nu = 2383.75$ cm^{-1}, m = 4, $\Delta\nu = 2.0$ cm^{-1})
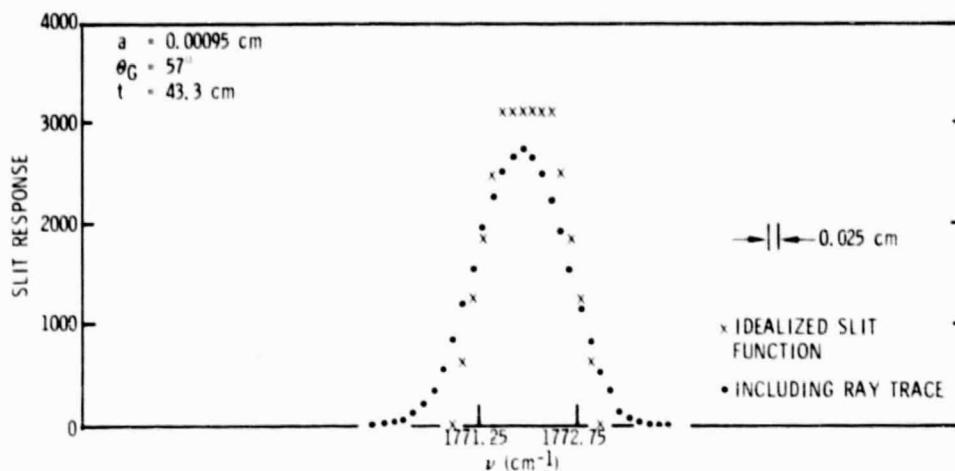
Figure 5. Slit Response Function ($\nu = 1772 \ cm^{-1}$, $m = 3$, $\Delta\nu = 1.5 \ cm^{-1}$)
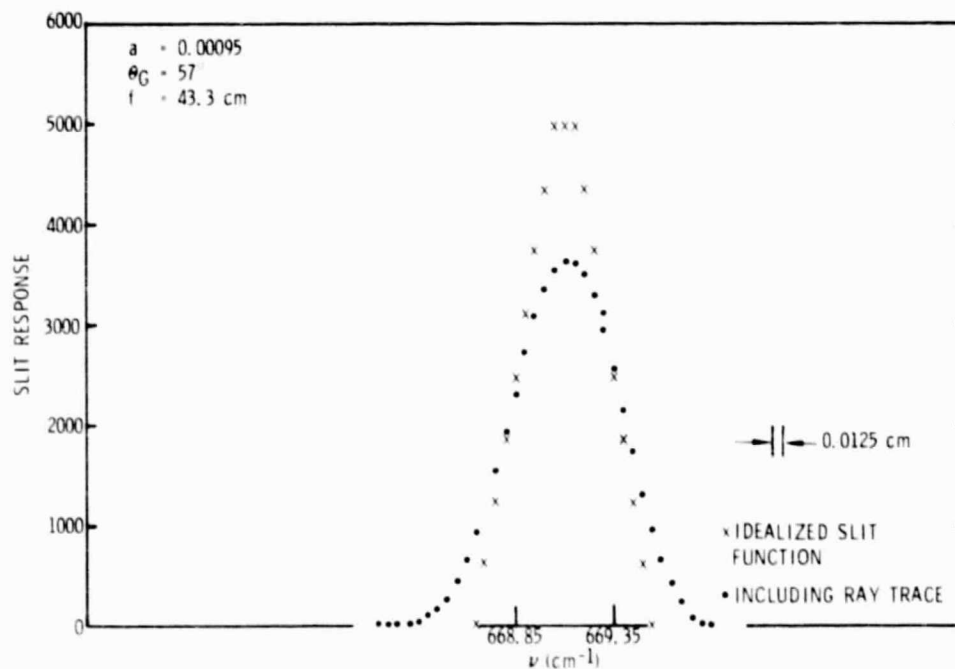
Figure 6. Slit Response Function ($\nu = 669.1 \ cm^{-1}$, $m = 1$, $\Delta\nu = 0.5 \ cm^{-1}$)
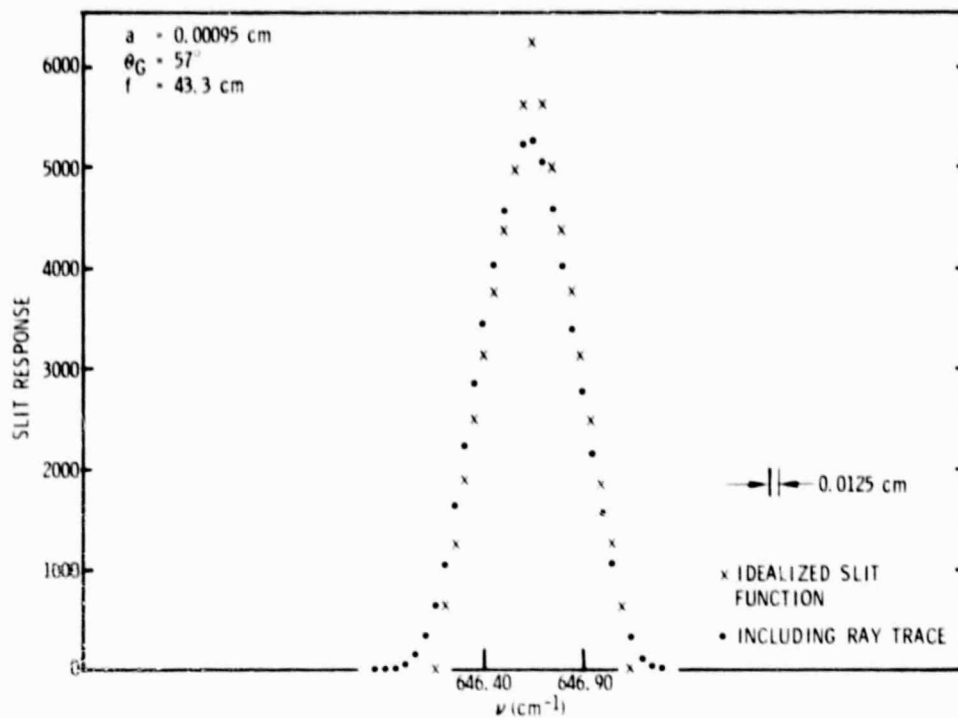
Figure 7. Slit Response Function ($\nu = 646.65$ cm^{-1}, m = 1, $\Delta\nu = 0.5$ cm^{-1})
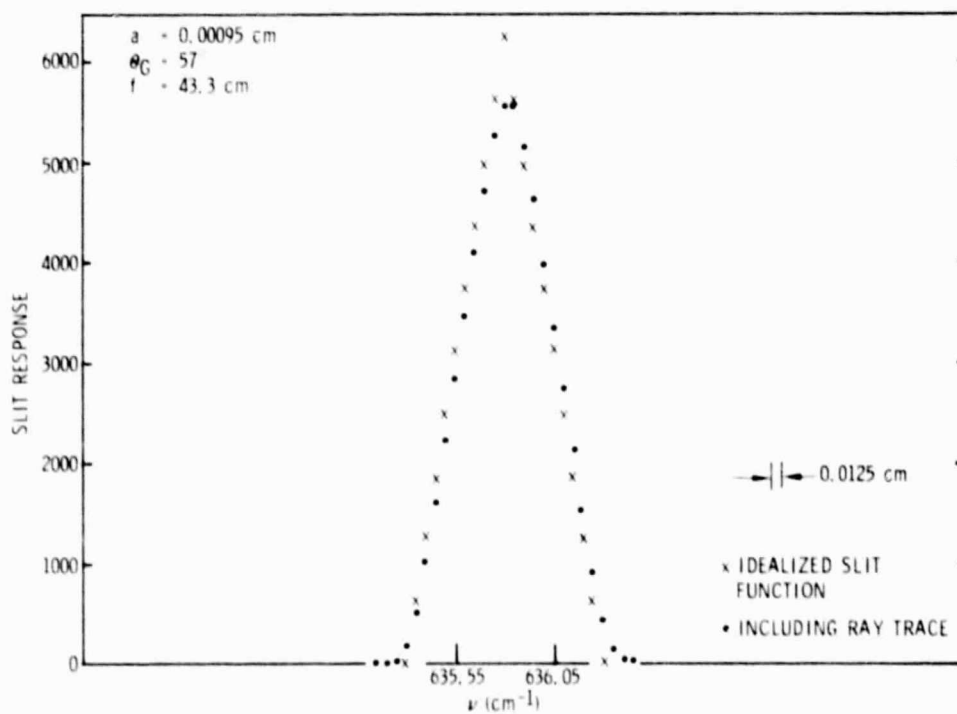
Figure 8. Slit Response Function ($\nu = 635.8$ cm^{-1}, m = 1, $\Delta\nu = 0.5$ cm^{-1})

SANTA BARBARA RESEARCH CENTER

14

DETECTOR PERFORMANCE

Background Calculation

Detector performance will be dependent to some extent on the background photon flux. This calculation together with those that follow will reveal how much detector and instrument cooling will be required.

There are three sources for photons which fall on the detector. These are the scene at temperature T_S, the instrument at temperature T_I, and the detector package at temperature T_d.

$$Q_{SCENE} = N_p(T_S, \Delta\nu_n)\Omega_{ES}\tau_S \text{ photons-sec}^{-1}\text{-cm}^{-2}$$

$$Q_{INST} = N_p(T_I, \Delta\nu_o)\Omega_{ES}(1 - \tau_S) \text{ photons-sec}^{-1}\text{-cm}^{-2}$$

$$Q_{DET} = N_p(T_d, \Delta\nu_w)(\pi - \Omega_{ES}) \text{ photons-sec}^{-1}\text{-cm}^{-2}$$

where N_p is the photon radiance for a given temperature T and spectral bandwidth

T_S, T_I, T_d are scene, instrument and detector temperatures, respectively

$\Delta\nu_n, \Delta\nu_o, \Delta\nu_w$ are, respectively, the inband, order filter, and wideband* spectral bandpasses

τ_S is the system optical transmittance

Ω_{ES} is the solid angle subtended by the exit slit at the detector and $(\pi - \Omega_{ES})$ is the solid angle of view of the detector excluding the exit slit.

Table 6 gives the photon flux from each of these sources for several representative channels. The scene temperature is assumed to be $300°K$.

Table 6 shows that background photons from the instrument dominate except for the coldest instrument temperatures and short wavelength channels where scene radiance dominates. The table also gives background limited (D^*_{BLIP}) for these conditions.

Table 7 is a compilation of three other noise sources expressed as D^*. These are: D^*_T, due to thermally generated hole-electron pairs; D^*_{JN} due

---

*Wideband means over the full spectral range to which the detector is sensitive.

to Johnson noise of the detector itself; and D^*_{PA} due to the noise voltage of the preamplifier.

Table 6. Background Photon Flux - Grating Spectrometer

T_{INST} (°K)	ν (cm⁻¹)	Q_{SCENE} (P-sec⁻¹-cm⁻²)	Q_{INST} (P-sec⁻¹-cm⁻²)	Q_{DET} (AT 90°K) (P-sec⁻¹-cm⁻²)	Q_{TOTAL} (P-sec⁻¹-cm⁻²)	D^*_{BLIP} (HgCdTe) (cm-Hz$^{\frac{1}{2}}$-watt⁻¹)
300	607	6.8×10^{13}	9.2×10^{15}	3.8×10^{14}	9.6×10^{15}	3.38×10^{11}
	1203	3.06×10^{13}	3.9×10^{15}	1.26×10^{12}	3.93×10^{15}	2.8×10^{11}
	1809.5	5.66×10^{12}	7.0×10^{14}	4.77×10^{7}	7.06×10^{14}	4.4×10^{11}
	2616	4.1×10^{11}	4.2×10^{13}	5.4×10^{5}	4.2×10^{13}	--
250	607	6.8×10^{13}	5.1×10^{15}	3.8×10^{14}	5.5×10^{15}	4.4×10^{11}
	1203	3.06×10^{13}	1.22×10^{15}	1.26×10^{12}	1.25×10^{15}	4.96×10^{11}
	1809.5	5.66×10^{12}	1.2×10^{14}	4.77×10^{7}	1.26×10^{14}	1.04×10^{12}
	2616	4.1×10^{11}	3.3×10^{12}	5.4×10^{5}	3.7×10^{12}	--
200	607	6.8×10^{13}	2.1×10^{15}	3.8×10^{14}	2.5×10^{15}	6.6×10^{11}
	1203	3.06×10^{13}	2.1×10^{14}	1.26×10^{12}	2.4×10^{14}	1.1×10^{12}
	1809.5	5.66×10^{12}	8.6×10^{12}	4.77×10^{7}	1.4×10^{13}	3.1×10^{12}
	2616	4.1×10^{11}	7.2×10^{10}	5.4×10^{5}	4.8×10^{11}	--

Table 7. Component HgCdTe Detectivities

DETECTOR TEMPERATURE (°K)	λ (µm)	λ_c (µm)	η	R (kv/watt)	r (Ω)	D^*_T (cm-Hz$^{\frac{1}{2}}$-watt⁻¹)	D^*_{JN} (cm-Hz$^{\frac{1}{2}}$-watt⁻¹)	D^*_{PA} (cm-Hz$^{\frac{1}{2}}$-watt⁻¹)
90	16.5	17	0.6	12	120	6.5×10^{10}	2×10^{12}	1.94×10^{12}
85	16.5	17	0.6	12	120	9.57×10^{10}	2.06×10^{12}	1.94×10^{12}
80	16.5	17	0.6	12	120	1.45×10^{11}	2.13×10^{12}	1.94×10^{12}
90	8.3	9	0.6	44	370	1.57×10^{12}	4.2×10^{12}	7×10^{12}
85	8.3	9	0.6	44	370	2.92×10^{12}	4.3×10^{12}	7×10^{12}
80	8.3	9	0.6	44	370	5.85×10^{12}	4.4×10^{12}	7×10^{12}
90	5.5	6	0.6	60	450	7.2×10^{13}	5.2×10^{12}	9.7×10^{12}
85	5.5	6	0.6	60	450	1.7×10^{14}	5.3×10^{12}	9.7×10^{12}
80	5.5	6	0.6	60	450	4.7×10^{14}	5.5×10^{12}	9.7×10^{12}

WHERE λ - WAVELENGTH OF OPERATION η - QUANTUM EFFICIENCY   r - DETECTOR RESISTANCE
λ_c - CUTOFF WAVELENGTH   R - DETECTOR RESPONSIVITY

These four component detectivities for photoconductive HgCdTe are given by the following expressions:

1. Background photon flux (Table 6)

$$D^*_{BLIP} = \frac{\lambda}{2hc}\left(\frac{\eta}{Q_B}\right)^{\frac{1}{2}}$$

2. Thermally generated noise

$$D^*_T = 5.3 \times 10^{10} \frac{\lambda}{\lambda_c}\left(\frac{hc}{e\lambda_c}\right)^{-\frac{3}{2}} (T_d)^{-\frac{7}{4}} e^{hc/2\lambda_c k T_d}$$

SANTA BARBARA RESEARCH CENTER

3. Johnson noise in the detector resistance

$$D^*_{JN} = \frac{R(A_D \Delta f)^{\frac{1}{2}}}{(4KT_d r_D)^{\frac{1}{2}}}$$

4. Preamplifier voltage noise

$$D^*_{PA} = \frac{R(A_D \Delta f)^{\frac{1}{2}}}{V_n}$$

The system D^* is given by

$$D^*_S = \left[\frac{1}{\left(\dfrac{1}{D^*_{BLIP}}\right)^2 + \left(\dfrac{1}{D^*_T}\right)^2 + \left(\dfrac{1}{D^*_{JN}}\right)^2 + \left(\dfrac{1}{D^*_{PA}}\right)^2} \right]^{\frac{1}{2}}$$

Combined system detectivities for the HgCdTe detectors are given in Table 8.

Table 8. HgCdTe System Detectivities

DETECTOR TEMPERATURE (°K)	λ (μm)	D° (cm-Hz$^{\frac{1}{2}}$-watt^{-1}) AT T_{INST}		
		300°K	250°K	200°K
90	16.5	6.3×10^{10}	6.4×10^{10}	6.5×10^{10}
85	16.5	9.2×10^{10}	9.3×10^{10}	9.4×10^{10}
80	16.5	1.3×10^{11}	1.4×10^{11}	1.4×10^{11}
90	8.3	2.7×10^{11}	4.7×10^{11}	8.7×10^{11}
85	8.3	2.8×10^{11}	4.8×10^{11}	9.8×10^{11}
80	8.3	2.8×10^{11}	4.9×10^{11}	1.0×10^{12}
90	5.5	4.4×10^{11}	1×10^{12}	2.6×10^{12}
85	5.5	4.4×10^{11}	1×10^{12}	2.6×10^{12}
80	5.5	4.4×10^{11}	1×10^{12}	2.6×10^{12}

These data show that cooling the instrument is effective in increasing D^* only in the short-wavelength channels whereas cooling the detector below $90°K$ is useful only for the long-wavelength channels. For optimum system performance, however, the instrument should be cooled below $250°K$ and the detector below $90°K$.

The expressions for photovoltaic InSb are as follows:

$$D^* - \frac{(A_D \Delta f)^{\frac{1}{2}}}{NEP_\lambda} = \frac{e(A_D \Delta f)^{\frac{1}{2}} \eta \lambda}{I_N \, hc}$$

The noise current I_N is the RSS of background photon noise, load resistor Johnson noise, and detector Johnson noise currents.

$$I_N = (I_{BN}^2 + I_{LRN}^2 + I_{JN}^2)^{\frac{1}{2}}$$

$$I_{BN} = (2\eta e^2 Q_B A_D)^{\frac{1}{2}}$$

$$I_{LRN} = \left(\frac{4KT_{LR}}{r_{LR}}\right)^{\frac{1}{2}}$$

$$I_{JN} = \left(\frac{4KTA_D}{\overline{RA}}\right)^{\frac{1}{2}}$$

where Q_B is obtained from Table 6.

The quantities used in the equations above are defined as follows:

D^* Detector detextivity, $cm\ Hz^{\frac{1}{2}}/watt$

λ Wavelength, cm

λ_c Detector cutoff wavelength

η Quantum efficiency, assumed to be 0.6

h   Planck's constant, 6.626196×10^{-34} joule sec

c   Velocity of light, 2.997925×10^{10} cm/sec

e   Electron charge, $1.6021917 \times 10^{-19}$ coulomb

T_d Detector temperature, K

k   Boltzmann's constant, 1.380622×10^{-23} joule/$^\circ$K

Q_B Photon flux density incident on detector, photons/sec cm^2

R   Responsivity, volts/watt

Δf Noise bandwidth, Hertz

r_D Detector resistance, ohms

V_N Preamplifier noise, volts/$\sqrt{Hz}$

A_D Detector area, $0.03318\ cm^2$

$\overline{RA}$ Detector resistance area product, 10^4 ohms cm^2

r_{LR} Load resistor, 10^9 ohms

InSb Detector Performance

The expected performance for the InSb detectors at 5.5-µm band below is summarized in Table 9. All of the D^* values shown are background limited (BLIP) except for the three values at the bottom (3.8 µm at 200°K) which are limited by the detector resistance-area product.

Table 9. InSb Detector Performance

T_{DET} (°K)	λ (µm)	$\overline{RA}$ (Ω-cm^2)	Q_B (P-cm^2-sec^{-1})	D° (cm-Hz$^{\frac{1}{2}}$-watt^{-1}) AT T_{INST}		
				300°K	250°K	200°K
90	5.5	3×10^4	7×10^{14}	5.7×10^{11}		
85	5.5	7×10^4	7×10^{14}	5.7×10^{11}		
80	5.5	1×10^5	7×10^{14}	5.73×10^{11}		
90	5.5	6.5×10^4	1.26×10^{14}		1.34×10^{12}	
85	5.5	1.5×10^5	1.26×10^{14}		1.34×10^{12}	
80	5.5	3.5×10^5	1.26×10^{14}		1.34×10^{12}	
90	5.5	1.5×10^5	1.4×10^{13}			3.9×10^{12}
85	5.5	4×10^5	1.4×10^{13}			4×10^{12}
80	5.5	10^6	1.4×10^{13}			4×10^{12}
90	3.8	1.5×10^5	4.2×10^{13}	2.3×10^{12}		
85	3.8	5×10^5	4.2×10^{13}	2.3×10^{12}		
80	3.8	10^6	4.2×10^{13}	2.3×10^{12}		
90	3.8	1.6×10^5	3.7×10^{12}		6.98×10^{12}	
85	3.8	5×10^5	3.7×10^{12}		7.6×10^{12}	
80	3.8	10^6	3.7×10^{12}		7.7×10^{12}	
90	3.8	1.7×10^5	4.8×10^{11}			1.3×10^{13}
85	3.8	5×10^5	4.8×10^{11}			1.7×10^{13}
80	3.8	1.3×10^6	4.8×10^{11}			1.96×10^{13}

SYSTEM PERFORMANCE

The D* values given in Tables 8 and 9 were used to calculate the NEN values shown in Table 10 using the following expression:

$$NEN = \frac{F_c \sqrt{A_D \Delta f_n} \times 10^7}{\Omega A \tau_T D^* \Delta \nu}$$

where F_c = 2.5 chopping factor

A_D = Table 5

ΩA = 0.01 solid angle-area product

τ_T = 0.21 total optical transmittance

$\Delta \nu$ = Table 1 spectral bandpass

Δf = 1.94 Hz (Table 2)

Table 10 gives the system NEN values for three instrument temperatures: 300°K, 250°K and 200°K and two detector temperatures: 90°K and 80°K. Also given in the table are signal-to-noise ratios for the maximum and minimum temperatures specified in Table 1. The data show that for a nominal instrument temperature of 250°K and detector temperature of 90°K the SNR = 100 is obtained except for channels 20, 27 and 28. In these latter two it can be argued that since the short-wavelength channels see deep in the atmosphere, the minimum temperature should be warmer than 214°K. For colder instrument or detector temperatures, performance is improved.

For the higher altitude free flyer application at 900 km the field of view can be reduced to give the same 45 km × 45 km footprint and the aperture increased to maintain the same AΩ. Under these conditions, Table 2 shows that the dwell time is reduced by a factor of about two. Thus, NEN values for the free flyer will be about a factor of 1.4 larger than those shown in Table 10.

Table 10. Grating Spectrometer NEN/SNR

INIT TEMP DETECTOR TEMP NEN IN ERGS	300K 90K	90K	250K 90K	80K	200K 90K	80K
607 SNR	6.45595 E-2	3.12865 E-2	6.35508 E-2	2.90518 E-2	6.26187 E-2	0.029073
288 216	2099.2 736.578	4311.04 1519.92	2122.36 748.27	4642.66 1636.84	2153.95 759.409	4639.27 1635.65
623.23 SNR	6.28886 E-2	3.04768 E-2	6.19058 E-2	2.82999 E-2	6.09535 E-2	2.82999 E-2
276 214	1951.33 704.9	3820.2 1454.56	1980.71 716.089	4114.06 1566.44	1910.1 727.278	4114.06 1566.44
627.75 SNR	6.24029 E-2	3.02414 E-2	6.04828 E-2	2.80813 E-2	6.04828 E-2	2.80813 E-2
246 213	1232.28 684.889	2542.8 1423.58	1271.4 711.79	2738.4 1533.09	1271.4 711.79	2738.4 1533.09
635.8 SNR	6.16673 E-2	2.98849 E-2	6.07039 E-2	2.77503 E-2	5.97698 E-2	2.77503 E-2
230 212	947.743 672.451	1955.66 1397.6	962.786 683.125	2106.1 1494.34	977.83 693.799	2106.1 1494.34
646.65 SNR	6.06726 E-2	2.94029 E-2	5.97246 E-2	2.73027 E-2	5.88059 E-2	2.73027 E-2
228 210	912.217 634.73	1882.25 1320.08	926.696 649.894	2027.15 1421.62	941.176 660.039	2027.15 1421.62
652.75 SNR	6.01691 E-2	2.91599 E-2	5.92235 E-2	2.70761 E-2	5.82221 E-2	2.70317 E-2
229 207	926.601 595.65	1912.03 1229.2	941.309 605.145	2059.11 1323.75	957.587 615.61	2062.5 1325.93
66.2 SNR	5.79491 E-2	2.80345 E-2	5.69452 E-2	2.60731 E-2	5.70794 E-2	2.65012 E-2
233 009	1011.48 626.742	2087.19 1293.28	1027.54 636.69	2247.74 1392.76	1025.12 635.142	2207.95 1368.11
666.4 SNR	5.88915 E-2	2.85397 E-2	5.79713 E-2	2.65012 E-2	5.69792 E-2	2.64546 E-2
233 204	992.344 614.591	2047.69 1269.2	1008.1 624.347	2205.21 1365.76	1025.65 635.217	2209.09 1368.16
668.1 SNR	5.88915 E-2	2.85397 E-2	5.79713 E-2	2.65012 E-2	5.66285 E-2	2.63847 E-2
254 220	1402.09 773.244	2843.19 1545.56	1424.34 785.523	3115.75 1718.33	1452.48 801.319	3129.5 1725.92
669.1 SNR	5.86326 E-2	2.84143 E-2	5.77165 E-2	2.63847 E-2	5.65034 E-2	0.026373
242 213	1160.86 670.053	2395.43 1382.65	1179.29 680.694	2579.7 1494.01	1148.25 641.631	2580.94 1494.67
1203 SNR	7.59672 E-3	7.31877 E-3	4.35833 E-3	4.18044 E-3	2.35958 E-3	2.05283 E-3
320 216	12288.8 405.04	12743.9 433.56	21391.6 1579.44	22301.4 1642.48	39512.1 2904.97	43841.2 3244.74
1231.8 SNR	7.42117 E-3	7.15613 E-3	4.26323 E-3	4.08922 E-3	2.30312 E-3	2.00372 E-3
320 216	11842.4 819.843	12291. 850.213	20614.6 1427.14	21491.8 1487.87	39158.9 2641.73	43860.9 3036.48
1272 SNR	3.16994 E-3	3.16994 E-3	1.39477 E-3	1.39477 E-3	5.36451 E-4	5.36451 E-4
250 216	778.495 156.346	778.495 156.346	1769.31 355.331	1769.31 355.331	4600.2 923.86	4600.2 923.86
1344.5 SNR	3.04733 E-3	3.04733 E-3	1.34082 E-3	1.34082 E-3	5.15124 E-4	5.15124 E-4
250 216	601.752 113.169	601.752 113.169	1367.62 257.203	1367.62 257.203	3559.79 669.477	3559.79 669.477
1399.5 SNR	2.96666 E-3	2.96666 E-3	1.30533 E-3	1.30533 E-3	5.02051 E-4	5.02051 E-4
250 216	512.056 92.5495	512.056 92.5495	1165.58 210.451	1165.58 210.451	3030.52 547.173	3030.52 547.173
1409.5 SNR	3.10366 E-3	3.10366 E-3	1.36561 E-3	1.36561 E-3	5.25235 E-4	5.25235 E-4
250 216	682.315 132.454	682.315 132.454	1550.72 301.031	1550.72 301.031	4031.86 782.68	4031.86 782.68
1514.4 SNR	4.02643 E-3	4.02643 E-3	1.77195 E-3	1.77195 E-3	6.82122 E-4	6.82122 E-4
270 216	1018.75 87.8656	1018.75 87.8656	2315.34 199.695	2315.34 199.695	6014.23 518.718	6014.23 518.718

Table 10. Grating Spectrometer NEN/SNR (Cont)

INIT TEMP	300K		250K		200K	
DETECTOR TEMP	90K	80K	90K	80K	90K	80K
NEN IN ERGS						
1950.9	3.03593 E-3	3.03593 E-3	1.33581 E-3	1.33581 E-3	5.13774 E-4	5.13774 E-4
SNR						
180	1841.82	1841.22	4195.95	4195.95	10883.5	10883.5
216	109.44	104.44	249.977	249.977	649.941	649.941
1930.1	2.90768 E-3	2.90768 E-3	1.27938 E-3	1.27938 E-3	4.92069 E-4	4.92069 E-4
SNR						
320	5015.22	5015.22	11398.2	11398.2	29635.4	29635.4
216	76.8377	76.8377	174.631	174.631	454.041	454.041
2383.75	6.02226 E-4	6.02226 E-4	1.97874 E-4	1.79886 E-4	7.99107 E-5	7.99107 E-5
SNR						
237	139.021	139.021	423.109	465.419	1047.7	1047.7
214	29.35	29.35	89.326	98.2596	221.189	221.189
2386.1	4.46907 E-4	4.46907 E-4	1.46841 E-4	1.33492 E-4	7.90681 E-5	7.90681 E-5
SNR						
257	571.956	571.956	1740.43	1914.48	3232.23	3232.23
214	39.0456	39.0456	118.835	130.718	220.693	220.693
2388.2	4.50087 E-4	4.50087 E-4	1.47886 E-4	1.34442 E-4	7.96028 E-5	7.96028 E-5
SNR						
274	1289.76	1289.76	3925.36	4317.9	7292.52	7292.52
215	41.2991	41.2991	125.693	138.262	233.512	233.512
2390.2	4.485 E-4	4.485 E-4	1.47364 E-4	1.33967 E-4	7.935 E-5	7.935 E-5
SNR						
292	2783.48	2783.48	8471.45	9319.6	15732.7	15732.7
215	40.9971	40.9971	124.774	137.251	231.723	231.723
2392.35	4.485 E-4	4.485 E-4	1.47364 E-4	1.33967 E-4	7.935 E-5	7.935 E-5
SNR						
306	4735.7	4735.7	14413.	15854.3	26767.	26767.
217	46.9633	46.9633	142.932	157.225	265.445	265.445
2394.5	4.485 E-4	4.485 E-4	1.47364 E-4	1.33967 E-4	7.935 E-5	7.935 E-5
SNR						
306	4700.71	4700.71	14306.5	15737.2	26569.3	26569.3
217	46.4235	46.4235	141.289	155.419	262.394	262.394
2424.2	3.96284 E-4	3.96284 E-4	1.30208 E-4	1.18371 E-4	7.01118 E-5	7.01118 E-5
SNR						
320	7905.12	7905.12	24059.1	26465.	44681.1	44681.1
214	35.7416	35.7416	108.779	119.657	202.018	202.018
2505	3.83403 E-4	3.83403 E-4	1.25975 E-4	1.14523 E-4	6.78329 E-5	6.78329 E-5
SNR						
320	6269.	6269.	19079.6	20987.5	35433.5	35433.5
214	23.6764	23.6764	72.0585	79.2643	133.823	133.823
2616.5	3.67598 E-4	3.67598 E-4	1.20782 E-4	1.09802 E-4	6.50366 E-5	6.50366 E-5
SNR						
320	4513.29	4513.29	13736.1	15109.7	25509.9	25509.9
214	13.2974	13.2974	40.4704	44.5174	75.1593	75.1593

PRELIMINARY GRATING SPECTROMETER
DETECTOR ARRAY CONFIGURATION

A principal concern in the design of the multidetector grating spectrom-
eter is the size of the detector array and the difficulty likely to be encountered
in cooling it. While cooling for the Space Shuttle application should not be a
problem since adequate supplies of gaseous nitrogen for a Joule-Thomson
cryostat or liquid nitrogen for a liquid transfer system can be carr'ed for
the anticipated two-week mission.

However, for the free flyer mission radiative cooling is probably the
most practical approach since the only reasonable alternative, a cryogenic
refrigerator, could require up to 100 watts of input power most of which
(~ 90 watts) would have to be dissipated radiatively. Although these devices
are currently under development for extended space missions (at Hughes the
VM cycle refrigerator) demonstrated reliability and service life are not yet
competitive with radiative coolers.

For purposes of this study we have found that the radiative cooler cur-
rently being developed for the Thematic Mapper to be flown on LANDSAT D
is a good baseline design for the AMTS. The spacecraft applications appear
to be similar with about the same orbit altitude (900 km) and sun orientation
(both are sun synchronous at ~ 10 am). Also, the detector heat loads appear
to be similar.

The size of the detector array on the AMTS is determined by the spec-
trometer focal length and dispersion angle β between detectors at the extreme
ends of the array (channels 10 and 15). For the system described the array
length will be 20.6 cm and the overall package size might be about $22 \times 2 \times 4$ cm
including the spherical field lens slivers and condensing light pipes. The en-
tire package will have to be cooled although only the detectors themselves will
need to be cooled to $90^\circ K$ or below. Using the design equations for the The-
matic Mapper (modified for the AMTS) and assuming that the detectors are
mounted on the cold stage of the radiative cooler and the lens/light pipe assem-
bly is mounted on the intermediate stage, the expected temperature for the

detectors is 77°K and for the intermediate stage is 131°K. A comparison of heat loads and operational temperatures between the Thematic Mapper and the AMTS is given in Table 11. Two figures showing schematic and perspective views of the Thematic Cooler are Figures 9 and 10, respectively.

Table 11. Low Orbit Radiant Cooler Nominal Heat Loads (All power in milliwatts)

HEAT SOURCE	TO INTERMEDIATE STAGE		TO COLD STAGE	
	TM (154°K)	AMTS (131°K)	TM (81.6°K)	AMTS (80.4°K)
INPUT RADIATION				
SPACECRAFT EMISSION	48	24	0.7	.4
EARTH EMISSION	33	33	5.5	5.5
EARTH ALBEDO	84	84	4.6	4.6
SOLAR SCANNER (FROM DOOR)	101(S)	--	0.7	--
DOOR EMISSION	369	185	--	--
SHIELD EMISSION	--	--	14.3	7.6
WARM STAGE EMISSION (INTERIOR)	1359	680	26.7	14.0
BAND AND LEAD PENETRATION	--	--	2.0	1.1
SCENE EMISSION (APERTURE)	--	--	4.2	11.7
CONDUCTION				
INTERSTAGE SUPPORTS	133	110	8.2	7.0
ELECTRICAL CABLING				
HEATER	47	39	11.6	10.0
OTHER	17	14	6.5	2.5
CONTAMINATION BARRIER	26	21	--	--
SUBSTRATE BIAS				
HgCdTe	--	--	4.4	15.0
InSb	--	--	10.8	15.0
TOTAL INPUT	2217	1190	100.2	94.4
OUTPUT				
RADIATOR (TO SPACE)	2090	1111	100.2	94.4
SHIELD (TO SPACE)	61	31	--	--
HOUSING (TO COLD STAGE)	--	--	--	--
RADIATION	52	27	--	--
CONDUCTION	14	21	--	--
TOTAL OUTPUT	2217	1190	100.2	94.4

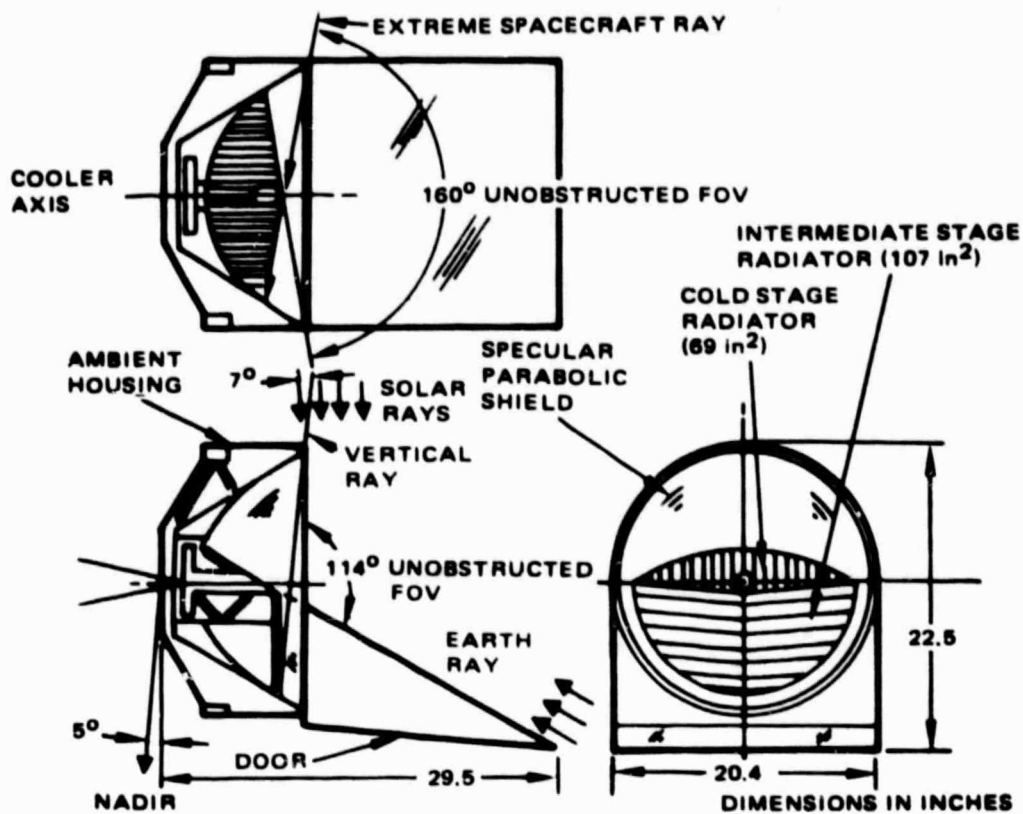(S) = SCATTERED RADIATION   TM AMBIENT STAGE = 300°K   AMTS AMBIENT STAGE = 250°K
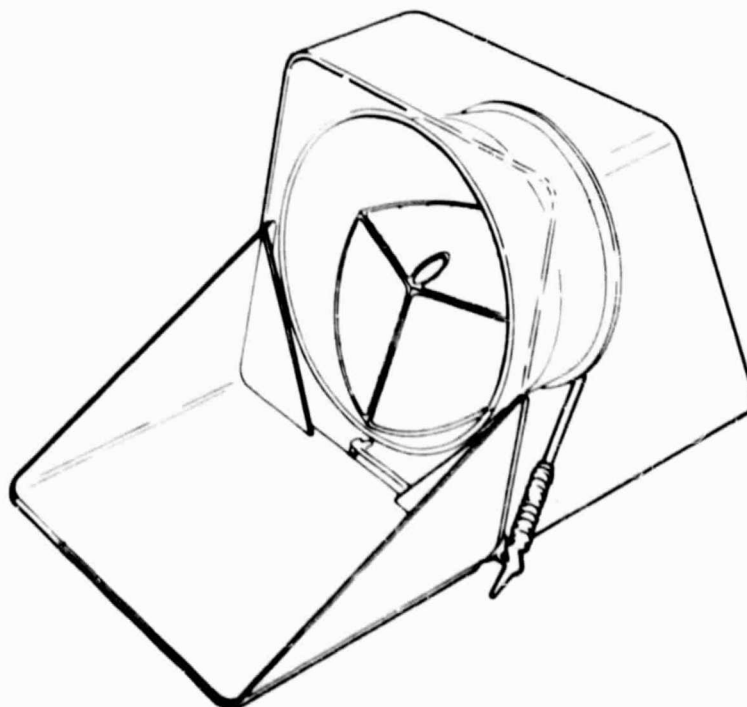
Figure 9. Cooler Schematic Showing Field of View

Figure 10. Perspective View of Radiant Cooler

SANTA BARBARA RESEARCH CENTER

MICHELSON INTERFEROMETER APPROACH

The reasons for pursuing the interferometer approach were as follows:

1. To reduce the overall instrument size and weight for the eventual free-flyer application.

2. To reduce the number of detectors requiring cooling. The interferometer to be described uses one InSb and two HgCdTe detectors.

3. To have the potential of higher throughput, spectral resolution and flexibility of channel selection as compared with the grating spectrometer.

The candidate interferometer is a 1-inch aperture flat-plate Michelson with the moving mirror attached to a rotating rather than translating assembly.

The advantages of this configuration are that the fringe output of the interferometer is not disturbed by first-order displacements or tilts of the moving mirror assembly. Also, since the moving assembly can be mounted on flex pivots an integral torquer can be used for drive thus eliminating the bearing and lubrication problems associated with a linear drive. Interferometric alignment tolerances still must be maintained between the two mirrors in the fixed and the two mirrors in the moving assemblies. Figure 11 shows the current configuration being developed at SBRC using the AMTS requirements as the baseline. The purpose of this effort is to develop the technology needed for future sounding applications.

Optical System

The instantaneous field of view (IFOV) of the interferometer is limited by the internal divergence angle and the spectral resolution ($R\Omega = 2\pi$). For most sounding channels the resolution is about 1200. Thus, the IFOV is 0.072 rad giving a footprint of 30 km × 30 km from Shuttle altitude without optical correction. However, the fore optics shown in Figure 11 allow demagnification so that a 45 km × 45 km footprint can be obtained independent of altitude
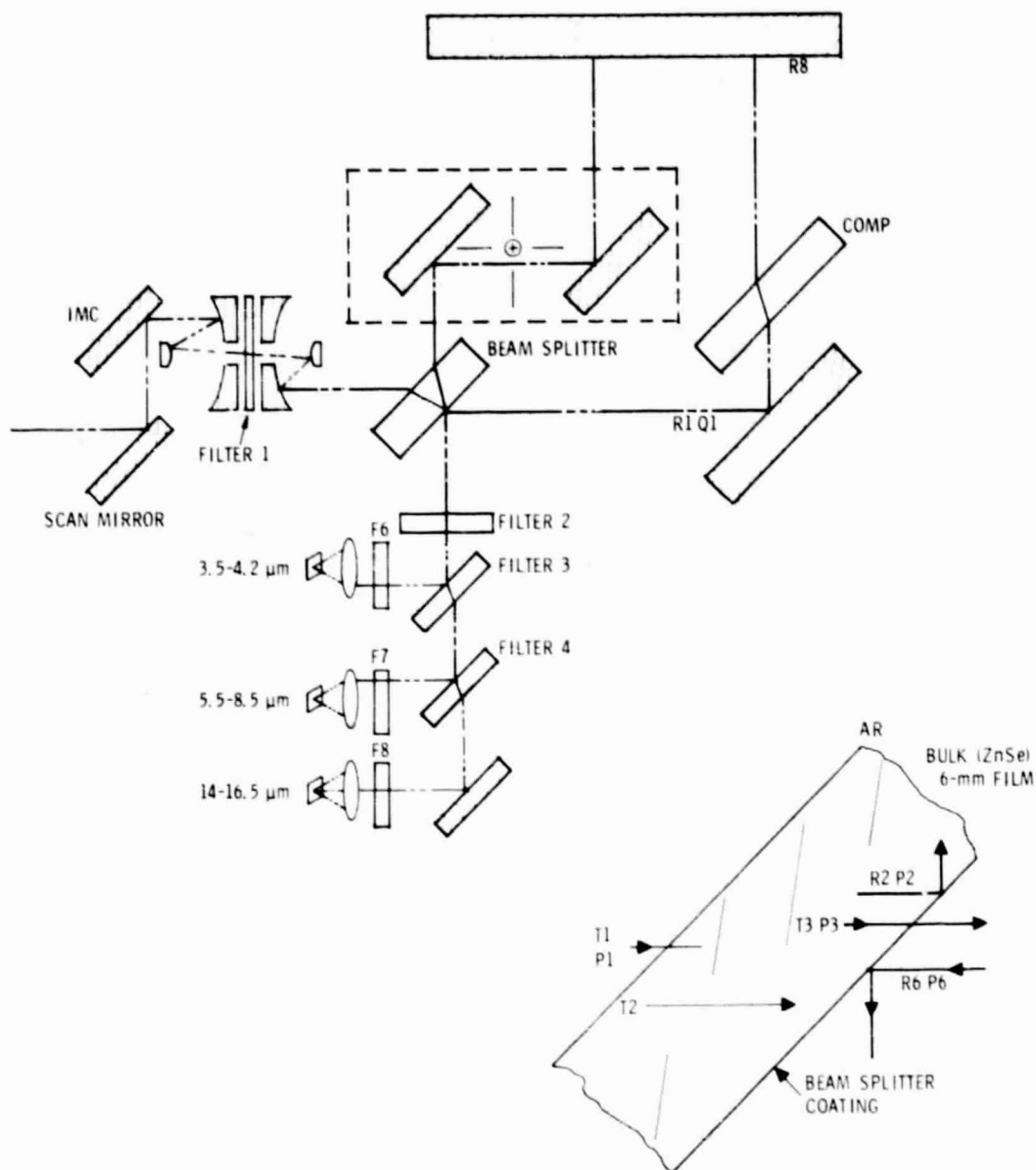
Figure 11. Michelson Interferometer Schematic

while maintaining constant AΩ. The stop in the fore optics provides a field defining aperture which will reduce the amount of stray light entering the interferometer.

The orbital parameters shown in Table 2 apply to the interferometer as well as to the grating instrument. The calculations for dwell time and noise bandwidth include a value of 60% for scan efficiency — which takes into account both the scan efficiency of the object-space scan system and the Michelson

mirror drive. In this system the object-space scan mirror moves in steps equal to the footprint and dwells at each step for a time equal to the dwell time shown in Table 2. The down track smear during the dwell time amounts to about 4% of the footprint dimension. This smear might not be a problem were it not for the fact that the 28 channels have various spectral resolutions. This means that the lower resolution channels are sampled at a smaller Michelson mirror deflection than the high resolution channels and thus at a different time.

Image motion compensation would correct for this problem directly. The amount of compensation required would be 3.7° per scan line.

Optical Parameters

The optical transmittance of the interferometer system depends on the properties of each element shown in Figure 11. Table 12 identifies each optical element which in some cases is characterized by transmittances for each of two polarization axes. Table 13 gives values of reflectance and transmittance for each optical element.

System transmittances are presented in Table 14.

Table 12. Optical Element Identification

S WAVE	P WAVE	DESCRIPTION
F1		TRANSMITTANCE FOR FILTER 1
F2		2
F3	P7	3
F4	P8	4
F5		5
F6		6
F7		7
F8		8
L1		TRANSMITTANCE FOR LENS 1
L2		2
L3		3
R1	Q1	REFLECTANCE FOR MIRROR AT 45
R2	P2	REFLECTANCE BEAM SPLITTER FILM FROM SUBSTRATE SIDE
R3	P5	REFLECTANCE FOR FILTER 3
R4	P9	REFLECTANCE FOR FILTER 4
R6	P6	REFLECTANCE BEAM SPLITTER FILM FROM AIR SIDE
R8		REFLECTANCE FOR MIRROR AT NORMAL
T1	P1	TRANSMITTANCE FOR BEAM SPLITTER AR COATING
T2		TRANSMITTANCE FOR BEAM SPLITTER (6 mm) SUBSTRATE
T3	P3	TRANSMITTANCE FOR BEAM SPLITTER (6 mm) AIR SIDE
K		FACTOR FOR FRINGE MODULATION DUE TO OPTICS FIGURE

Table 13. Optical Element Characteristics

F3	P7	F4	P8	F5	F6	F7	F8	R8
0.75	0.75	0.80	0.80	0.99	0.75	0.70	0.60	0.98 *

L1	L2	L3	R1	Q1	R3	P5	R4	P9
0.98	0.95	0.98	0.99	0.97	0.90	0.90	0.85	0.85 *

C#	T1	P1	R2	P2	T3	P3	R6	P6	T2	F1	K
1	0.95	0.99	0.48	0.48	0.52	0.81	0.46	0.19	0.91	0.80	1.00
2	0.95	0.99	0.48	0.48	0.52	0.81	0.46	0.19	0.91	0.80	1.00
3	0.96	0.99	0.48	0.48	0.52	0.81	0.46	0.20	0.91	0.80	1.00
4	0.96	0.99	0.48	0.48	0.52	0.81	0.47	0.20	0.91	0.80	1.00
5	0.96	0.99	0.49	0.49	0.51	0.81	0.47	0.21	0.91	0.80	1.00
6	0.96	0.99	0.49	0.49	0.51	0.79	0.48	0.21	0.91	0.80	1.00
7	0.97	0.99	0.49	0.49	0.51	0.79	0.48	0.22	0.92	0.80	1.00
8	0.97	0.99	0.50	0.50	0.50	0.78	0.49	0.22	0.92	0.80	1.00
9	0.97	0.99	0.50	0.50	0.50	0.78	0.49	0.23	0.92	0.80	1.00
10	0.97	0.99	0.50	0.50	0.50	0.77	0.49	0.23	0.92	0.80	1.00
12	0.93	0.99	0.66	0.66	0.34	0.67	0.61	0.33	0.99	0.90	1.00
19	0.97	0.99	0.60	0.60	0.40	0.63	0.58	0.37	0.99	0.90	1.00
28	0.95	0.99	0.38	0.47	0.62	0.53	0.36	0.47	0.99	0.90	1.00

*Values are wavelength independent

C# Means up to and including the channel number specified.

Table 14. System Optical Parameters

C#	V	T1	T2	AC	FO	AO	TOTAL BACK	SIG	(S-P)/(S+P)
1	607.00	0.22	0.13	0.17	0.71	0.28	0.072	0.035	-.05
2	623.23	0.22	0.13	0.17	0.71	0.28	0.072	0.035	-.05
3	625.75	0.23	0.14	0.18	0.71	0.29	0.075	0.037	-.04
4	635.80	0.23	0.14	0.18	0.71	0.29	0.076	0.037	-.03
5	646.65	0.23	0.14	0.18	0.71	0.29	0.077	0.037	-.05
6	652.75	0.23	0.14	0.18	0.71	0.29	0.076	0.037	-.04
7	666.20	0.23	0.15	0.19	0.71	0.30	0.082	0.040	-.03
8	666.90	0.23	0.15	0.19	0.71	0.30	0.082	0.040	-.03
9	668.10	0.23	0.16	0.19	0.71	0.30	0.083	0.040	-.04
10	669.10	0.23	0.15	0.19	0.71	0.30	0.082	0.040	-.03
11	1203.00	0.27	0.17	0.22	0.80	0.36	0.128	0.062	-.25
12	1231.80	0.27	0.17	0.22	0.80	0.36	0.128	0.062	-.25
13	1772.00	0.26	0.20	0.23	0.80	0.39	0.145	0.072	-.11
14	1844.50	0.26	0.20	0.23	0.80	0.39	0.145	0.072	-.11
15	1889.50	0.26	0.20	0.23	0.80	0.39	0.145	0.072	-.11
16	1809.50	0.26	0.20	0.23	0.80	0.39	0.145	0.072	-.11
17	1839.40	0.26	0.20	0.23	0.80	0.39	0.145	0.072	-.11
18	1850.90	0.26	0.20	0.23	0.80	0.39	0.145	0.072	-.11
19	1930.10	0.26	0.20	0.23	0.80	0.39	0.145	0.072	-.11
20	2383.75	0.20	0.19	0.20	0.80	0.59	0.186	0.093	-.05
21	2386.10	0.20	0.19	0.20	0.80	0.59	0.186	0.093	-.05
22	2388.20	0.20	0.19	0.20	0.80	0.59	0.186	0.093	-.05
23	2390.20	0.20	0.19	0.20	0.80	0.59	0.186	0.093	-.05
24	2392.35	0.20	0.19	0.20	0.80	0.59	0.186	0.093	-.05
25	2394.50	0.20	0.19	0.20	0.80	0.59	0.186	0.093	-.05
26	2424.00	0.20	0.19	0.20	0.80	0.59	0.186	0.093	-.05
27	2505.00	0.20	0.19	0.20	0.80	0.59	0.186	0.093	-.05
28	2616.50	0.20	0.19	0.20	0.80	0.59	0.186	0.093	-.05

Where:

T1 = Interferometer arm 1 transmittance

T2 = Interferometer arm 2 transmittance

AC = Interferometer signal transmittance

FO = Transmittance of fore optics

AO = Transmittance of aft optics

Total Back = $(T_1+T_2)(AO)(FO)$ = total system transmittance for background radiation

Sig = $\sqrt{T_1 T_2}$ = total system transmittance for signal (AC part of interferogram)

(S-P)/(S+P) = Amount of polarization

Background Photon Flux

The photon flux falling on the detectors originates from two principal sources: the scene, and the instrument itself. That portion coming from the instrument is a function of the emissivity of the optics. From Table 14 it is clear that the emission of the aft optics dominates and therefore the temperature of this assembly is important. For the systems calculations that follow it is assumed that the detectors, cold stops and cold filters/dichroics are held at $90°$K and the rest of the aft optics at $150°$K (cold and intermediate stage temperatures of a Thematic Mapper type cooler).

While the interferometer has a throughput advantage as compared to the grating instrument the detectors see a greater background photon flux not only from the increased throughput but also because the detectors must operate broadband. Moreover, the interferometer offers no multiplex advantage. To obtain optimum performance it is necessary to cold-shield the detectors in such a way as to minimize the background on the short-wavelength detectors. The channels are therefore separated into three spectral groups as follows:

Channels	Frequency	Detector Type
1-10	$607-669$ cm^{-1}	HgCdTe
11-19	$1203-1930.1$ cm^{-1}	HgCdTe
20-28	$2383.75-2616.5$ cm^{-1}	~~HgCdTe~~ InSb

The aft optics condensing lens will be 1-inch diameter f/1. The detector will therefore be 1.83×1.83 mm. The background photon fluxes and expected detectivities for the three spectral ranges are given in Table 15.

Table 15. Background and Detectivity

FREQUENCY (cm^{-1})	Q_B (P-sec^{-1}-cm^{-2})	D* (cm-Hz$^{1/2}$-watt^{-1})		D* LIMITED BY	
		AT 90 K	AT 80 K	90 K	80 K
607-669 (HgCdTe)	1.29×10^{16}	5×10^{10}	8×10^{10}	THERMAL GENERATION	BACKGROUND
1203-1930.1 (HgCdTe)	2.9×10^{15}	5×10^{11}	7×10^{11}	BACKGROUND	BACKGROUND
2383.75-2616.5 (InSb)	5.8×10^{13}	7×10^{12}	9×10^{12}	DETECTOR JOHNSON NOISE	

BACKGROUND CALCULATED FROM 220 K SCENE + 250 K INSTRUMENT + 150 K AFT OPTICS

The noise equivalent radiance (NEN) values shown in Table 16 were calculated using the expression:

$$NEN = \frac{\sqrt{A_D \Delta f} \times 10^7}{\Omega A\, T_o\, D^* \Delta \nu}$$

where A_D = detector area = 0.0334 cm^2

Δf = $1/(2\,T_p)$ related to $\Delta \nu$; see Table 2

$A\Omega$ = 0.026

T_o = See Table 14

D^* = See Table 15

$\Delta \nu$ = See Table 1

Table 16. Interferometer NEN and SNR Values

CH#	FREQ	NEN(90)	T1	SNR(T1)	T2	SNR(T2)	T(100/1 SNR)	D*
1	607.00	0.11724	288	1150	216	406	216	5 E+10
2	623.23	0.11724	276	993	214	378	214	5 E+10
3	625.75	0.11090	246	695	213	390	213	5 E+10
4	635.80	0.11090	230	527	212	374	212	5 E+10
5	646.65	0.11090	228	499	210	350	210	5 E+10
6	652.75	0.11090	229	503	207	323	207	5 E+10
7	666.20	0.10259	233	570	209	353	209	5 E+10
8	666.90	0.10259	233	570	209	353	209	5 E+10
9	668.10	0.10259	254	805	220	444	220	5 E+10
10	669.10	0.10259	242	663	213	383	213	5 E+10
11	1203.00	0.00468	320	19921	216	1467	216	5 E+11
12	1231.80	0.00468	320	18779	216	1300	216	5 E+11
13	1772.00	0.00329	250	750	216	151	216	5 E+11
14	1844.50	0.00329	250	557	216	105	216	5 E+11
15	1889.50	0.00329	250	462	216	83	220	5 E+11
16	1809.50	0.00329	250	644	216	125	216	5 E+11
17	1839.40	0.00329	270	1247	216	108	216	5 E+11
18	1850.90	0.00329	280	1699	216	101	216	5 E+11
19	1930.10	0.00329	320	4432	216	68	223	5 E+11
20	2383.75	0.00016	237	531	214	112	214	7 E+12
21	2386.10	0.00016	257	1622	214	111	214	7 E+12
22	2388.20	0.00016	274	3684	215	118	215	7 E+12
23	2390.20	0.00016	292	7922	215	117	215	7 E+12
24	2392.35	0.00016	306	13478	217	134	217	7 E+12
25	2394.50	0.00016	306	13379	217	132	217	7 E+12
26	2424.00	0.00014	320	22241	214	101	214	7 E+12
27	2505.00	0.00014	320	17053	214	64	220	7 E+12
28	2616.50	0.00014	320	11771	214	35	228	7 E+12

Where NEN(90°) is the value calculated with an instrument temperature of 250°K, aft optics temperature of 150°K, and a detector temperature of 90°K

T1 = maximum specified scene temperature

T2 = minimum specified scene temperature

T(100/1 SNR) = scene temperature for SNR = 100
if SNR(T2) < 100

DATA REQUIREMENTS

The data requirements for the two systems are similar provided that the interferogram processing is done on-board and in such a way as to produce the same 28 discrete channel outputs as does the grating spectrometer.

If the 28 data channels are multiplexed and linearly digitized, the number of bits required to digitize the dynamic range defined by the minimum and maximum specified temperatures is given in Table 17. The number of bits is chosen such that the digitization level is equal to the NEΔT. The rms temperature uncertainty ΔT_s, therefore, will be given by:

$$\Delta T_s = \frac{NEN}{[\partial N/\partial T]} \left(1 + \frac{1}{\sqrt{12}}\right) \,^\circ K$$
$$T_1, T_2$$

and the number of bits required:

$$n = \frac{\log[N(T_2) - N(T_1)]}{\log 2} \qquad \Delta N = N(T_2) - N(T_1)$$

Table 17 shows the resultant system temperature uncertainty ΔT_s for both systems. Generally, the grating instrument is better by a factor of two.

If a 16-bit digitizer were used for all channels, the percentage improvement would be as shown in Table 17.

Table 17. System Temperature Uncertainty and Data Bit Requirements

CHANNEL NO.	ΔN (ergs/etc.)	BITS (n)[*]	GRATING		INTERFEROMETER		% IMPROVEMENT USING 16 BITS
			ΔT_S (K)	ΔT_S (K)	ΔT_S (K)	ΔT_S (K)	
1	87.32	11	0.0547	0.0903	0.101	0.167	0.9
2	72	11	0.0559	0.0905	0.106	0.171	0.9
3	33.85	10	0.066	0.089	0.121	0.164	0.45
4	16.98	9	0.076	0.091	0.139	0.167	0.22
5	16.53	9	0.076	0.093	0.142	0.172	0.22
6	19.9	9	0.075	0.096	0.141	0.180	0.22
7	22.2	9	0.0698	0.091	0.126	0.164	0.22
8	22.2	9	0.071	0.093	0.126	0.165	0.22
9	37	10	0.059	0.081	0.105	0.144	0.45
10	28.8	13	0.066	0.088	0.116	0.157	3.6
11	86.4	15	0.003	0.022	0.004	0.024	14.4
12	81.8	15	0.0046	0.023	0.004	0.026	14.4
13	1.97	11	0.018	0.066	0.042	0.157	0.9
14	1.49	11	0.022	0.088	0.054	0.216	0.9
15	1.25	10	0.025	0.105	0.064	0.265	0.45
16	1.71	11	0.011	0.077	0.048	0.185	0.9
17	3.75	12	0.015	0.114	0.028	0.211	1.8
18	5.26	12	0.0089	0.090	0.022	0.222	1.8
19	14.4	14	0.0043	0.0043	0.011	0.319	7.2
20	0.066	9	0.050	0.192	0.040	0.153	0.22
21	0.238	11	0.0142	0.144	0.015	0.155	0.9
22	0.562	12	0.0072	0.138	0.008	0.147	1.8
23	1.23	14	0.0037	0.139	0.004	0.148	7.2
24	2.10	14	0.0024	0.124	0.003	0.132	7.2
25	2.11	14	0.0024	0.096	0.003	0.133	7.2
26	3.12	15	0.0016	0.155	0.002	0.168	14.4
27	2.39	15	0.0019	0.234	0.002	0.294	14.4
28	1.65	14	0.0025	0.388	0.003	0.452	7.2

[*]n - NUMBER OF BITS FOR THE GRATING SPECTROMETER CASE

SUMMARY

The results of this study show that instrumentation for high resolution sounding of the atmosphere is feasible. In terms of present day technology the baseline grating spectrometer approach appears to be preferable to the interferometer approach since it gives a factor of about two better NEN performance in all channels. However, there are other tradeoffs to consider which may shift the balance toward the interferometer. These are discussed below.

Size and Weight

The grating instrument will occupy a volume roughly 60 by 25 by 25 cm and will weigh about 120 pounds, not including electronics or cooler. This compares with an estimate of 30 by 30 by 25 cm and weight of 80 pounds for the interferometer. Since detector cooling requirements for the interferometer are less than for the grating instrument, the overall difference in size and weight will be even greater.

Sensitivity

Table 17 gives a comparison of temperature uncertainty, ΔT_s, for the two systems. For the conditions assumed, the grating system is a factor of approximately two better in all channels. Some improvement is possible for the interferometer by careful design of optical element coatings, but the total improvement would be at most about 25%. Additional improvement is possible by increasing the aperture.

Spectral Channel Selection

The channel wavelengths for the grating instrument are determined by the detector location in the dispersion plane and are fixed by the design, although by rocking the grating, all channels can be scanned up or down in frequency to some extent. Due to physical interference of the detectors, none of the channels can overlap. The interferometer on the other hand has complete flexibility as to channel frequency and bandwidth, and, of course, a complete spectrum can be produced if desired.

Spatial Scanning

The scan mirror in the grating spectrometer scans cross course in a continuous motion. When a footprint 45 km × 45 km has been scanned by the image of the entrance slit, all channels are held, sampled by the multiplexer, and digitized sequentially. Thus, the output of each spectral channel is integrated over the 45-km footprint.

The interferometer uses two mirrors: one to step scan the 45-km × 45-km footprint cross course, and the other to compensate for the down-course motion during the Michelson mirror travel.

Mechanical Complexity

As mentioned in the previous section, the interferometer scan is more complicated than the grating instrument scan, and although the flex pivot mounted Michelson mirror assembly is simple and insensitive to first order tilts, mechanical alignment and stability are of the utmost importance. Off-setting this to some extent is the need in the grating instrument for a grating "rocker" to maintain alignment between the grating and the dispersion plane, and for spectral calibration purposes. In addition, the grating instrument has a chopper mechanism which can be a simple resonant fork device.

Data Processing

The grating system is clearly simpler than the interferometer since no on-board processing is needed and the data rate is low. However, it lacks the potential flexibility of the interferometer.

Several data processing methods are possible for the interferometer. One method, using a phase lock loop analyzer currently under development at SBRC, operates basically like a wave analyzer, producing sine, cosine, and $\sin^2+\cos^2$ outputs for each spectral channel. Like the grating instrument, individual channel outputs are produced but the spectral placement can be commanded remotely, and there is no restriction on overlapping channels.

The conventional Fast-Fourier Transform method using an on-board special-purpose computer may be feasible in the time scale of this flight, particularly if simplifications in the algorithm can be effected.

Of course, the interferogram can be sampled directly and the data sent to the ground at a high data rate. In this case, the complete spectrum would be available.

Detector Cooling

For the Shuttle application, either system could use a Joule-Thomson cryostat or liquid transfer system. However, for the TIROS type spacecraft, radiative cooling is appropriate. The cooling capability of the Thematic Mapper cooler currently under development at SBRC appears adequate for the grating instrument, but a somewhat smaller design would be satisfactory for the interferometer.